Association of Fractal Geometry and Data Augmentation Through GANs and XAI for Classification of Histology Images

Vinicius Augusto Toreli Borgue[1][a], Bianca Lançoni de Oliveira Garcia[1][b], Sérgio Augusto Pelicano Júnior[1][c], Guilherme Freire Roberto[2][d], Guilherme Botazzo Rozendo[3][e], Leandro Alves Neves[1][f], Alessandro Santana Martins[4][g], Thaína Aparecida Azevedo Tosta[5][h] and Marcelo Zanchetta do Nascimento[6][i]

[1]*Department of Computer Science and Statistics (DCCE), Sao Paulo State University (UNESP), São José do Rio Preto, Brazil*

[2]*Institute of Mathematics and Computer Science (ICMC), University of São Paulo (USP), Sao Carlos, Brazil*

[3]*Department of Computer Science and Engineering (DISI), University of Bologna, Cesena, Italy*

[4]*Federal Institute of Triângulo Mineiro (IFTM), Ituiutaba, Brazil*

[5]*Federal University of São Paulo (UNIFESP), São José dos Campos, Brazil*

[6]*Faculty of Computer Science (FACOM), Federal University of Uberlândia (UFU), Uberlândia, Brazil*

{*vinicius.borgue, bianca.lanconi, s.pelicano, leandro.neves*}*@unesp.br*, {*guilhermefroberto, marcelo.zanch azzo@unibo.it*

Keywords: Generative Adversarial Networks, Explainable Artificial Intelligence, Handcrafted Fractal Features, Histology Images.

Abstract: In computer vision, one of the main challenges regarding the classification of histopathology images lies on the low number of samples available in public image datasets. For the past year, the most common approaches applied to handle this problem consisted of using geometric data augmentation to increase the dataset size. Recently, the use of GANs to generate artificial images to increase the size of the training set for the classification of histology images has been proposed. Despite obtaining promising results in the deep learning context, there has not yet been much research regarding the use of these approaches in the context of handcrafted features. In this paper, we propose the use of handcrafted features based on fractal geometry and GANs for data augmentation for classifying four histology image datasets. The GANs were assisted by explainable artificial intelligence (XAI) to enhance the quality of the generated images. The fractal features obtained from the original and artificial images were given as input to six classifiers. After analyzing the results, we verified that, despite obtaining the best overall performance, our method was only able to provide a slight improvement in two datasets.

1 INTRODUCTION

With the advancement of high-resolution whole-slide scanning equipment, pathology laboratories have adopted the digitization of hematoxylin and eosin (H&E) stained tissue sections for tissue analysis, aiding in disease identification (Alajaji et al., 2023). The digitization of high-resolution whole slides enables the use of artificial intelligence (AI) techniques to improve the accuracy and speed of the diagnostic process, which is a time-intensive process that requires the full focus and attention of the pathologists. As discussed by (Rozendo et al., 2024), many studies highlight the challenge of training AI models to analyze histological images due to the limited number of labeled images available, owing to the high cost of annotation and patient data privacy concerns. The lack of labeled data can lead to model overfitting. To balance the number of images in different

[a] https://orcid.org/0009-0005-5855-5126
[b] https://orcid.org/0009-0007-3758-7457
[c] https://orcid.org/0009-0001-3724-4557
[d] https://orcid.org/0000-0001-5883-2983
[e] https://orcid.org/0000-0002-4123-8264
[f] https://orcid.org/0000-0001-8580-7054
[g] https://orcid.org/0000-0003-4635-5037
[h] https://orcid.org/0000-0002-9291-8892
[i] https://orcid.org/0000-0003-3537-0178

Borgue, V. A. T., Garcia, B. L. O., Pelicano Júnior, S. A., Roberto, G. F., Rozendo, G. B., Neves, L. A., Martins, A. S., Tosta, T. A. A. and Zanchetta do Nascimento, M. Association of Fractal Geometry and Data Augmentation Through GANs and XAI for Classification of Histology Images.
DOI: 10.5220/0013280200003929

In *Proceedings of the 27th International Conference on Enterprise Information Systems (ICEIS 2025) - Volume 1*, pages 756-762
ISBN: 978-989-758-749-8; ISSN: 2184-4992

classes, (Ryspayeva, 2023) proposed the use of generative adversarial networks (GANs) to generate synthetic images, demonstrating that the technique can improve model accuracy. In order to increase the amount of colorectal cancer histological images available for training, (Jiang et al., 2023) proposed the use of Multi-Scale Gradient (MSG-GANs) to generate synthetic images at different scales. The model generates synthetic images that are filtered by a selection mechanism to remove images with class ambiguity, leading to an improvement in the model accuracy from 86.87% to 89.54%. The generator network was optimized to produce images at various resolutions, ensuring high-quality generated images. Facing the same challenges, (Brancati and Frucci, 2024) proposed using GANs to increase the number of available breast tumor images for training. The proposed model uses Conditional GANs to generate synthetic images, not directly in terms of pixels but in terms of image features such as texture and shape, reducing computational costs while preserving important information. The use of fractal dimension (FD) has shown potential in quantifying the morphological complexity of brain tumours, providing a new method for glioma classification. The study by (Battalapalli et al., 2023) investigated the potential of FD as a biomarker for classifying low-grade and high-grade gliomas in magnetic resonance images where the model achieved an accuracy of 90% in classifying low-grade gliomas and 85% in classifying high-grade gliomas. Although the study did not explore histological images, the application of FD demonstrates the potential of fractal methods for extracting complex features. The proposed method incorporates fractal dimension to extract features from colorectal cancer histological images, generating synthetic images through GANs, which are used to train a classification model. Moreover, the the use of GANs assisted by explainable AI (XAI) tools for enhance the quality of the generated images has been explored successfully in (Rozendo et al., 2024), however, this approach has not yet been studied in association with handcrafted features.

The motivation behind this study arises from the need to increase the number of histological images available for training pathology classification models. The use of GANs to generate synthetic images has been applied as a solution to the problem of low availability of labeled data. Additionally, fractal dimension and its association with percolation theory have been explored as ways to extract complex features from histological images. The proposed method combines these techniques to improve the accuracy of pathology classification models. The expected contributions of this work are:

1. The extraction of handcrafted fractal features from histology GAN images;
2. Application of GANs as a data augmentation approach for histology datasets;
3. Association of XAI techniques and GAN to enhance the quality of the generated histology images.

Section 2 of the article describes the application of the proposed approach on the selected datasets and the details of the fractal feature extraction method as well as the generation of the artificial images. Then, in Section 3, the results are presented, along with a comparative performance analysis between different models. The conclusion is presented in Section 4.

2 MATERIAL AND METHODS

2.1 Datasets

The proposed approach was applied to four different datasets, which were representative of three different types of histological tissue: colorectal, breast and liver, which are exemplified in Figure 1. The original images were split into multiple patches with a 64×64 resolution without overlapping. The number of obtained patches as well as an overview of each dataset is presented in Table 1.

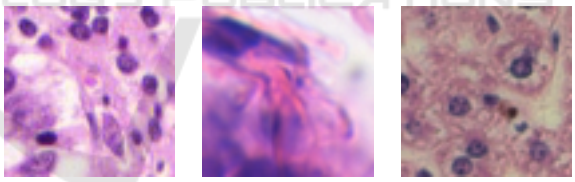

(a) (b) (c)

Figure 1: Samples from each type of histology tissue. (a) colorectal tissue; (b) breast tissue; (c) liver tissue.

2.2 Method Overview

Our proposed method consists of three different stages: first, artificial datasets are generated by training a GAN model using the original patches. Then, fractal dimension, lacunarity and percolation features are extracted from the original and artificial patches. Finally, the generated feature vectors are given as input to classical machine learning algorithms. An overview of the proposed approach is shown in Figure 2, and each stage of the method is explained in the following subsections.

Table 1: Overview of the evaluated datasets.

Dataset	Image	Classes	Samples	Patches
UCSB	Breast tumours	2	32+26	4,608+3,744
CR	Colorectal tumours	2	74+91	4,664+5,736
LG	Liver tissue	2	150+115	2,400+1,840
LA	Liver tissue	4	100+115+162+152	1,600+1,840+2,592+2,416

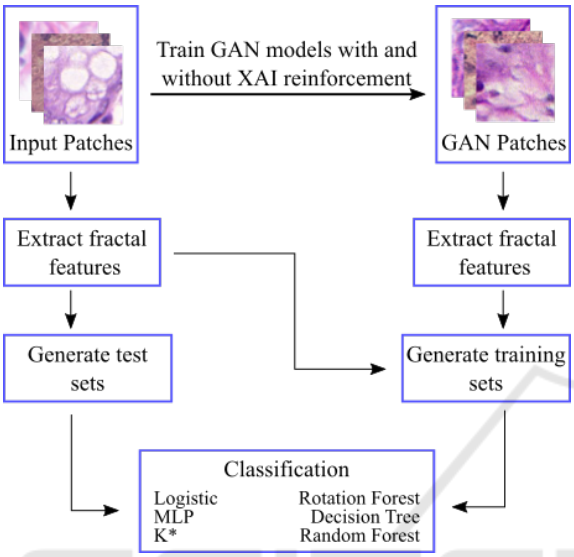

Figure 2: Overview of the proposed approach.

2.3 Generating Artificial Patches

To generate artificial patches, we employed a method called XGAN, which builds upon traditional Generative Adversarial Networks (GANs) by incorporating Explainable Artificial Intelligence (XAI) techniques.

In a standard GAN setup, the system comprises two main components: a generator (G) and a discriminator (D). The generator G is responsible for creating synthetic images, starting from a random input vector z. These generated images $G(z)$ are designed to resemble real data as closely as possible. The discriminator D, on the other hand, acts as a classifier that evaluates whether a given image is real (x, from the original dataset) or synthetic ($G(z)$, created by the generator). The generator improves its output iteratively by learning to "fool" the discriminator, while the discriminator simultaneously learns to distinguish real from fake.

The XGAN introduces an additional layer of intelligence to this interaction by leveraging XAI techniques to make the discriminator's decision-making process transparent. Instead of the generator merely relying on the discriminator's binary feedback (real or fake), it gains access to more detailed insights into why the discriminator made its decision. These insights, known as "explanations," highlight the features of the image that the discriminator found most important in making its classification.

By integrating these explanations (E) into the generator's training process, XGAN allows the generator to understand and focus on the features that are important for producing more realistic images. This feedback loop is formalized in a custom loss function ($\mathcal{L}_G^{ed}$), where the traditional adversarial loss ($\mathcal{L}_G^{adv}$) is combined with the XAI-derived explanations to refine the generator's output:

$$\mathcal{L}_G^{ed} = \mathcal{L}_G^{adv} \cdot E$$

For this work, we employed the RaSGAN (Relativistic Standard GAN) (Jolicoeur-Martineau, 2018) and WGAN-GP (Wasserstein GAN Gradient Penalty) (Gulrajani et al., 2017) models to establish the traditional adversarial loss functions. Additionally, we utilized XAI techniques, including Saliency (Simonyan et al., 2014), DeepLIFT (Shrikumar et al., 2019), and Gradient⊙Input (Hechtlinger, 2016), to generate the explanations (E) that guided the generator's refinement process. In Figure 3, a schematic of the proposed XGAN model is illustrated.

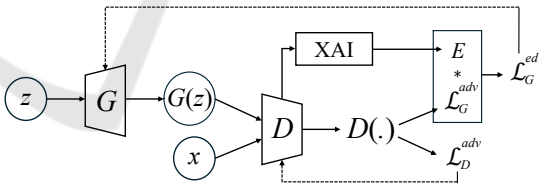

Figure 3: Schematic of the proposed XGAN model.

2.3.1 Adversarial Models

The loss function for the RaSGAN discriminator, denoted as $\mathcal{L}_D^{RaSGAN}$, was established as the combination of the DCGAN loss and the relativistic discriminator loss:

$$\mathcal{L}_D^{RaSGAN} = \mathcal{L}_D^{RaSGAN} + \mathcal{L}_{rel}$$

where the relativistic loss was defined as:

$$\mathcal{L}_{rel} = -\frac{1}{2}\mathbb{E}_{x\sim p(x), z\sim p(z)}\left[\log(D(x) - D(G(z)))\right].$$

As for the generator, the loss function $\mathcal{L}_G^{RaSGAN}$ was expressed as:

$$\mathcal{L}_G^{RaSGAN} = \begin{array}{l} -\frac{1}{2}\mathbb{E}_{z\sim p(z)}\left[\log(1-D(G(z)))\right] \\ -\mathbb{E}_{x\sim p(x)}\left[\log(D(x))\right] \end{array}$$

In our WGAN-GP approach, the loss function for the discriminator was formulated using the Wasserstein distance (L_W) along with a gradient penalty (L_{GP}):

$$L_D^{WGAN-GP} = -L_W + L_{GP}$$

In this formulation, L_W captured the difference in expected outputs from the discriminator for real and synthetic samples:

$$L_W = \mathbb{E}_{x\sim p(x)}[D(x)] - \mathbb{E}_{z\sim p(z)}[D(G(z))]$$

And the L_{GP} gradient penalty is represented as:

$$L_{GP} = \lambda \mathbb{E}_{\hat{x}\sim p(\hat{x})}[(\|\nabla_{\hat{x}} D(\hat{x})\|_2 - 1)^2]$$

where $\hat{x}$ denotes an interpolated sample created between real and generated data, and λ adjusts the strength of the penalty. For the generator, the loss function was given by the negative of the expected output from the discriminator for the generated samples:

$$L_{WGAN-GP}^G = -\mathbb{E}_{z\sim p(z)}[D(G(z))]$$

2.3.2 XAI Methods

To obtain the Saliency explanation ($E_{Saliency}$) for a generated image $G(z)$, we computed the gradient of the discriminator's output $D(G(z))$ with respect to the input $G(z)$:

$$E_{Saliency} = \frac{\partial D(G(z))}{\partial G(z)}.$$

To implement the DeepLIFT method, we evaluated the importance of input $G(z)$ by comparing its impact on the output with a baseline input x_0, which was set to minimal activation (zero). Denoting t as the output neuron and $\eta_1, \eta_2, \ldots, \eta_n$ as the neurons influencing t, we define the difference in output as $\Delta t = t - t_0$. The explanation $E_{DeepLIFT}$ is calculated as:

$$E_{DeepLIFT} = \sum_{i=1}^{n} C\Delta\eta_i \Delta t = \Delta t, \qquad (15)$$

where $\Delta\eta_i$ represents the change in activations for $G(z)$ versus x_0, and $C\Delta\eta_i\Delta t$ indicates how much $\Delta\eta_i$ contributes to Δt. Lastly, for the Gradient$\odot$Input explanation ($E_{Gradient\odot Input}$), we performed a multiplication of the gradients with the input values:

$$E_{Gradient\odot Input} = \frac{\partial D(G(z))}{\partial G(z)} \odot G(z).$$

2.3.3 Fractal Features

In order to obtain handcrafted features from both the original and artificial image sets, we apply the feature extraction techniques based on fractal geometry as described in (Roberto et al., 2021). The three types of fractal features extracted are: Fractal Dimension (FD), which is a metric that accounts for how much space is filled in a structure, such as an image; Lacunarity (LAC), which is a measure complementary to the FD, which accounts for how the space of a fractal is filled; and Percolation (PERC), which evaluates properties such as the distribution of cluster and the porosity of a structure. This is done by applying the multiscale and multidimensional approaches proposed by (Ivanovici and Richard, 2010). The multiscale approach consists in applying the gliding-box algorithm to evaluate all regions of the image at different scales, and the multidimensional approach consists in evaluating pixel similarity levels inside a given region sized $L \times L$, considering the intensity of the RGB color channels and the chessboard distance between each pixel and the center pixel of the region. The local and global features are then obtained, which results in a features vector composed of 100 local and 21 global features for each image.

2.3.4 Classification and Performance Evaluation

After obtaining all 121 features from the original and artificial patches of the four evaluated datasets, we prepared the training and test feature sets using a 10-fold cross validation approach. The classifications were performed on the Weka 3.8.6 platform. We chose six classifiers that were representative of the most common supervised learning approaches: Logistic (LOG), Multilayer Perceptron (MLP), K*, Rotation Forest (RoF), Decision Tree (DT) and Random Forest (Raf). All classifications were done using the algorithm's default parameters in Weka.

Since the datasets are not perfectly balanced, we chose to use the area under the ROC curve (AUC) as the evaluation metric. After classifying the feature sets from all GAN and XAI associations of the four datasets, we applied the Friedman's non-parametric test to verify the statistical significance of the obtained results (Japkowicz and Shah, 2011). This test was performed using the software Stats Direct.

3 RESULTS AND DISCUSSION

In this section, we present the results obtained from the application of our proposed approach. Firstly, we

present the AUC values obtained from the classification of all four tested datasets. Then, we present a statistical analysis using a non-parametric test. In all tables, the best results are highlighted in bold.

The first evaluation was performed on the UCSB dataset. The AUC values obtained from applying our approach to the original and generated patches are shown in Table 2. The best overall result was obtained using only the original patches and the LOG classifier, which provided an AUC value of 0.747. Regarding the application of our approach, the best result consisted of an AUC value of 0.740, which was also obtained with the LOG classifier and associating the WGAN-GP with the DeepLift explanation.

For the CR dataset, the best classification result was an AUC value of 0.802, which was obtained from the classification of the original patches using the RaF classifier. This classifier was able to provide the best AUC values in all of the nine evaluated scenarios for this dataset. When our approach was applied, the best result (0.799) was obtained using the RaSGAN with InputXGrad explanations. These results are shown in Table 3.

Finally, we evaluated the liver tissue datasets. For the LG dataset, as shown in Table 4, the best AUC value was obtained by applying our proposed method using the WGAN-GP and either the DeepLift or InputXGrad explanations. With these combinations, the AUC value of 0.924 was provided by the RaF classifier. As for the LA dataset, the results shown in Table 5 show that the highest AUC value was obtained when our approach was applied using the RaSGAN with Saliency explanations. This combination provided an AUC value of 0.912 using the MLP classifier.

In order to evaluate the statistical significancy of these results, we applied the non-parametric Friedman test to calculate the average rankings of each of the 54 tested combinations (classifier + GAN + explanation method). The average ranking of each of these combinations is shown in Table 6. The 10 highest rankings are highlighted in bold. The best average ranking was achieved using the RaF classifier with our approach by combining the RaSGAN and the InputXGrad explanations. In fact, the use of the InputXGrad explanations with the WGAN-GP was also able to provide the second best average ranking with the RaF classifier. All of the combinations evaluated with this classifier were ranked in the Top-10, which indicates that the RaF is able to consistently provide high AUC values for these datasets.

However, when we apply 2-sided Conover test to evaluate all pairwise comparisons between each of the tested combinations, we verified that the performance difference among the 10 best ranked treatments is not statistically significant considering $\alpha < 0.05$. For instance, the *p-value* obtained when comparing the combination that provided the best average ranking obtained using our proposed approach (RaF + RaSGAN + InputXGrad) and the one obtained using only the original images is $P_k = 0.638$. This indicates that, despite providing the best overall results, our method only slightly improves the results obtained when only the original patches are used.

4 CONCLUSION

In this work, we aimed to demonstrate the capabilities of handcrafted features combined with data augmentation, evaluating these methods for their potential to improve diagnostic accuracy in histological images. We applied two different types of Generative Adversarial Networks (GANs) to datasets of colorectal tissue (CR), breast tissue (UCSB), and liver tissue (LG and LA), and then compared the test results of various types of classic machine learning algorithms in the handcrafted features — as described in (Roberto et al., 2021) — extracted from the datasets, with and without artificial augmentation. Additionally, we evaluated the contribution of explainable AI methods applied during the generating phases and how they could influence the resulting accuracy comparison. To this end, RasGAN and WGAN-GP were implemented with different XAI methods during the generating phase: DeepLift, InputXGrad, and Saliency, as described in (Rozendo et al., 2024). Hence, to investigate whether the classic algorithms and GANs combined with handcrafted features can obtain competitive results in the classification of histological images — which is noted in brain magnetic resonance images (Battalapalli et al., 2023) — we conducted a comprehensive analysis on both original and augmented datasets. This allowed us to evaluate the impact of data augmentation on classification accuracy across multiple tissue types and algorithm combinations.

The results were solid regarding the usage of GANs, but the obtained AUC values suggest that the improvement obtained with data augmentation is minimal, occurring only in a few select combinations of datasets and algorithms. However, it fails to reach the same level of improvement observed with the use of GANs in (Jiang et al., 2023) and (Rozendo et al., 2024). Otherwise, the performance of the different classification algorithms regarding the presence of data augmentation generally remains equal. As observed in the UCSB dataset: the combination of WGAN-GP surpasses or is equal to both RasGAN and original implementations in RaF and MLP —

Table 2: AUC values obtained from the classification of the UCSB dataset.

UCSB	Original	RaSGAN				WGAN-GP			
		None	Deep Lift	Input XGrad	Saliency	None	Deep Lift	Input XGrad	Saliency
LOG	**0.747**	0.735	0.725	0.724	0.718	0.739	0.740	0.733	0.738
MLP	0.701	0.720	0.715	0.716	0.714	0.711	0.711	0.717	**0.722**
K*	**0.628**	0.626	0.625	0.626	0.625	0.619	0.619	0.625	0.624
RoF	0.729	**0.732**	0.727	0.726	0.723	0.726	0.724	**0.732**	0.726
DT	0.605	0.598	0.608	**0.617**	0.608	0.605	0.607	0.602	0.611
RaF	0.732	0.731	0.730	0.731	0.730	0.730	0.729	0.732	**0.733**

Table 3: AUC values obtained from the classification of the CR dataset.

CR	Original	RaSGAN				WGAN-GP			
		None	Deep Lift	Input XGrad	Saliency	None	Deep Lift	Input XGrad	Saliency
LOG	**0.786**	0.770	0.778	0.778	0.780	0.783	0.769	0.771	0.778
MLP	0.783	0.782	0.776	0.782	0.777	**0.785**	**0.785**	0.782	0.778
K*	**0.678**	0.676	0.677	0.677	**0.678**	0.677	0.672	0.674	0.674
RoF	0.788	0.788	0.789	**0.791**	0.789	0.789	0.789	0.787	0.784
DT	0.636	0.636	**0.643**	0.641	0.640	0.642	0.636	0.639	0.636
RaF	**0.802**	0.794	0.798	0.799	0.798	0.798	0.795	0.794	0.797

Table 4: AUC values obtained from the classification of the LG dataset.

LG	Original	RaSGAN				WGAN-GP			
		None	Deep Lift	Input XGrad	Saliency	None	Deep Lift	Input XGrad	Saliency
LOG	**0.922**	0.914	0.913	0.913	0.910	0.909	0.915	0.916	0.898
MLP	**0.922**	0.919	0.918	0.920	0.916	0.917	0.916	0.908	0.917
K*	0.828	**0.829**	**0.829**	**0.829**	**0.829**	**0.829**	**0.829**	**0.829**	**0.829**
RoF	0.922	0.921	0.920	0.921	0.918	0.921	**0.923**	0.918	0.918
DT	**0.777**	0.754	0.768	0.758	0.756	0.773	0.752	0.769	0.753
RaF	0.923	0.923	0.922	0.923	0.923	0.923	**0.924**	**0.924**	0.923

Table 5: AUC values obtained from the classification of the LA dataset.

LA	Original	RaSGAN				WGAN-GP			
		None	Deep Lift	Input XGrad	Saliency	None	Deep Lift	Input XGrad	Saliency
LOG	**0.898**	0.894	0.894	0.894	0.896	0.890	0.891	0.892	0.890
MLP	0.901	0.908	0.905	0.905	**0.912**	0.905	0.911	0.910	0.907
K*	0.817	0.817	0.817	**0.818**	**0.818**	**0.818**	**0.818**	0.817	**0.818**
RoF	**0.893**	0.891	0.892	0.892	0.891	0.889	0.891	0.888	0.889
DT	0.733	0.734	0.734	0.732	0.733	0.731	0.732	**0.736**	0.733
RaF	0.897	0.897	0.897	**0.899**	0.898	0.897	0.898	0.898	0.897

Table 6: Average rankings provided by the Friedman test for each tested combination.

	Original	RaSGAN				WGAN-GP			
		None	Deep Lift	Input XGrad	Saliency	None	Deep Lift	Input XGrad	Saliency
LOG	**10.8**	21.9	25.8	26.1	26.9	22.9	22.8	22.0	25.4
MLP	19.8	20.6	25.1	22.9	24.4	23.6	19.9	19.9	24.3
K*	40.6	41.0	41.1	40.5	39.4	40.9	42.1	42.0	41.4
RoF	17.1	17.4	18.6	18.0	21.8	20.8	18.1	20.4	23.9
DT	50.0	51.5	47.8	49.1	49.6	49.9	52.3	49.3	50.6
RaF	**8.4**	**11.0**	**11.9**	**7.6**	**9.4**	**10.5**	**9.6**	**8.0**	**8.9**

with Saliency — and in RoF — with InputXGrad —; the performance of LOG and K* is better in the original implementation; and RasGAN performs better in RoF and DT, with no XAI method and with InputXGrad respectively. A similar pattern can be noted in the CR dataset, with each type of augmentation performing better in the same number of algorithms, not following a specific pattern. However, the performance in the LG dataset is more pronounced, with RasGAN never providing the better results. Since our implementations performed equally well in the other two datasets, with no combination standing out, the results raise the question of whether data augmentation made a significant difference in these classifications at all. Additionally, the LG dataset generally suggests that between RasGAN and WGAN-GP, the

latter can be more competitive with the no augmentation implementation.

In essence, the potential of GANs to compensate for dataset difficulties, including or not XAI methods, is not very present here, and this can be for a variety of reasons, including the necessity of more intensive training in the generating phase. Nevertheless, this work is significant for the fractal features and histological images classification research, as it presents the results performance of using handcrafted features in histological images. These findings provide guidelines for researchers and experts interested in developing artificial augmentation techniques for histopathological datasets, and what to expect on the performance of these methods. The association of handcrafted features and data augmentation in histological images does not present itself in these cases, but since it should improve the results, there are a few lines to go from here.

In future work, we should evaluate different GAN training methods combined with handcrafted features. There's potential for augmentation to yield better results with more intensive training, compared to transformer and convolutional counterparts (Rozendo et al., 2024). While this might seem like a drawback, the time invested in fractal geometry analysis — which can be significantly shorter than more complex implementations in some cases — offsets this concern. Furthermore, the potential for combining fractal geometry analysis with other advanced machine learning techniques could lead to more robust and accurate classification models for histological images. As the field continues to evolve, it will be crucial to explore these hybrid approaches to maximize the benefits of both handcrafted features and new techniques.

ACKNOWLEDGEMENTS

This research was funded in part by the Coordenação de Aperfeiçoamento de Pessoal de Nível Superior—Brasil (CAPES)—Finance Code 001; National Council for Scientific and Technological Development CNPq (Grants #132940/2019-1, #313643/2021-0 and #311404/2021-9); the State of Minas Gerais Research Foundation—FAPEMIG (Grant #APQ-00578-18); São Paulo Research Foundation—FAPESP (Grant #2022/03020-1).

REFERENCES

Alajaji, S. A., Khoury, Z. H., Elgharib, M., Saeed, M., Ahmed, A. R., Khan, M. B., Tavares, T., Jessri, M., Puche, A. C., Hoorfar, H., et al. (2023). Generative adversarial networks in digital histopathology: current applications, limitations, ethical considerations, and future directions. *Modern Pathology*, page 100369.

Battalapalli, D., Vidyadharan, S., Prabhakar Rao, B., Yogeeswari, P., Kesavadas, C., and Rajagopalan, V. (2023). Fractal dimension: analyzing its potential as a neuroimaging biomarker for brain tumor diagnosis using machine learning. *Frontiers in Physiology*, 14:1201617.

Brancati, N. and Frucci, M. (2024). Improving breast tumor multi-classification from high-resolution histological images with the integration of feature space data augmentation. *Information*, 15(2):98.

Gulrajani, I., Ahmed, F., Arjovsky, M., Dumoulin, V., and Courville, A. (2017). Improved training of wasserstein gans.

Hechtlinger, Y. (2016). Interpretation of prediction models using the input gradient.

Ivanovici, M. and Richard, N. (2010). Fractal dimension of color fractal images. *IEEE Transactions on Image Processing*, 20(1):227–235.

Japkowicz, N. and Shah, M. (2011). *Evaluating learning algorithms: a classification perspective*. Cambridge University Press.

Jiang, L., Huang, S., Luo, C., Zhang, J., Chen, W., and Liu, Z. (2023). An improved multi-scale gradient generative adversarial network for enhancing classification of colorectal cancer histological images. *Frontiers in Oncology*, 13:1240645.

Jolicoeur-Martineau, A. (2018). The relativistic discriminator: a key element missing from standard gan.

Roberto, G. F., Lumini, A., Neves, L. A., and do Nascimento, M. Z. (2021). Fractal neural network: A new ensemble of fractal geometry and convolutional neural networks for the classification of histology images. *Expert Systems with Applications*, 166:114103.

Rozendo, G. B., Garcia, B. L. d. O., Borgue, V. A. T., Lumini, A., Tosta, T. A. A., Nascimento, M. Z. d., and Neves, L. A. (2024). Data augmentation in histopathological classification: An analysis exploring gans with xai and vision transformers. *Applied Sciences*, 14(18):8125.

Ryspayeva, M. (2023). Generative adversarial network as data balance and augmentation tool in histopathology of breast cancer. In *2023 IEEE International Conference on Smart Information Systems and Technologies (SIST)*, pages 99–104. IEEE.

Shrikumar, A., Greenside, P., and Kundaje, A. (2019). Learning important features through propagating activation differences.

Simonyan, K., Vedaldi, A., and Zisserman, A. (2014). Deep inside convolutional networks: Visualising image classification models and saliency maps.